Reconstruction of the Wenchuan debris flow process in August, 2022 by in-situ monitoring and analysis of seismic signals

Yan Yan[a,c], Renhe Wang[a], Cheng Zeng[a] , Yifei Cui[b]*, Sheng Hu[d], Xinglu Wang[a], Hui Tang[e]

[a] Key Laboratory of High-Speed Railway Engineering, MOE/School of Civil Engineering, Southwest Jiaotong University, Chengdu 610031, China

[b] State Key Laboratory of Hydroscience and Engineering, Tsinghua University, Beijing 100084, China

[c] Section 4.6: Geomorphology, German Research Centre for Geosciences (GFZ), Potsdam 14473, Germany

[d] College of Urban and Environmental Sciences, Northwest University, Xi'an 710127, China

[e] Section 4.7: Earth Surface Process Modelling, German Research Centre for Geosciences (GFZ), Potsdam 14473, Germany

*Corresponding author: Yifei Cui, e-mail: yifeicui@mail.tsinghua.edu.cn

Abstract

Rainfall-induced debris flows are highly destructive due to their abrupt onset, rapid movement, and high sediment transport capacity, all of which can lead to significant loss of life and damage to infrastructure. However, a comprehensive analysis of their dynamic evolution remains limited by the scarcity of in-situ monitoring data. In this study, we utilized near-field seismic data recorded by acquisition instruments deployed in Wenchuan, China, combined with images and post-event field investigations to reconstruct the second debris flow event in Fotangba Gully. Seismic signal attenuation was compensated, and time-frequency analysis and power spectral density (PSD) calculations were conducted. The results reveal pronounced differences in signal amplitude and frequency content across stations, reflecting spatial heterogeneity in flow dynamics. We identified flow velocity and grain concentration as the dominant factors affecting the PSD curves. This research provides a framework for extracting debris flow kinematics characteristics from seismic signals and offers new insights for hazard evaluation and the design of mitigation strategies.

Keywords: Debris flow seismic; Reconstruction; Kinematic characteristics; Wenchuan (China)

Highlights:

- By analyzing the characteristics of seismic signals, the study successfully reconstructed the entire process of the second debris flow event at Futangba Gully by utilizing features such as the time series, flow velocity, particle characteristics, and surge variations of the debris flow.
- The seismic signal characteristics of the debris flow showed rapid excitation and slow attenuation. Even after removing propagation effects, significant differences in amplitude and frequency were observed at different observation stations, indicating changes in the dynamic parameters of the debris flow.
- The time-frequency characteristics of seismic signals reflect the evolution process of debris flows, with a corresponding relationship between the power spectral density and debris flow characteristics.

1 Introduction

Debris flows are solid-fluid mixtures that can create destructive surges during heavy rainfall (Iverson, 1997). Recent incidents include a debris flow in Zhouqu County, China, on August 7, 2010, which caused 1,765 deaths and damaged over 5,500 homes (Tang et al., 2011), and another in Montecito, California, on January 9, 2018, resulting in 189 casualties and damage to 408 houses (Kean et al., 2019). Given the significant potential for disaster, measures to mitigate debris flows have attracted considerable attention. Existing methods for reducing debris flows include monitoring and early warning systems, risk assessment, and technical control technologies (Chen et al., 2015; Hürlimann et al., 2019; Chang et al., 2020). However, due to the complexity of debris flow dynamics and the incomplete understanding of the triggering mechanisms, these measures have certain limitations. For example, monitoring and early warning systems can trigger false alarms or overlook warnings, risk warnings can be inaccurate, and technical control measures can be either oversized or ineffective, leading to a waste of resources. Therefore, clarifying the complex process characteristics of debris flows is crucial to provide effective references for disaster management measures.

Current research on debris flow processes is primarily based on laboratory experiments, in situ monitoring, and field investigations (Marchi et al., 2002; Iverson, 2015; Hürlimann et al., 2019; Yang et al., 2021; He et al., 2022; Zhang et al., 2022). Although laboratory experiments allow various parameters (flow rate, slope, and material composition) to be controlled in order to simulate different debris flow movements and investigate their dynamic properties, they are limited by spatial and technical constraints (Yan et al., 2025). Therefore, these experiments cannot fully replicate the complexity and variability of natural environments, making it difficult to accurately reflect the actual dynamic processes of debris flows in the field. Field investigations of debris flows consist of pre- and post-event investigations. Pre-event investigations are primarily used to assess debris flow risk, while post-event investigations provide valuable first-hand data to understand the specific impacts of the

disaster, assess damage, analyze the extent and movement of debris flows, and investigate the underlying mechanisms of their occurrence. Field investigation methods include drone surveys, remote sensing images, and field investigation (Crowley et al., 2003; Liang et al., 2022; Turbessi et al., 2025). However, field investigations rely primarily on comparing traces before and after the debris flow to draw conclusions about the movement process. This requires preliminary investigations and, in addition, the disaster site must remain undisturbed after the event. Since debris flows occur suddenly and are often hidden, it is difficult to ensure that investigations were carried out before the event. Furthermore, without continuous data collection throughout the debris flow, there are no reliable data sets to validate the derived results, making it crucial to collect comprehensive data on the entire debris flow process. On-site monitoring plays a crucial role in understanding the triggering factors of debris flows (precipitation) and collecting important data (flow depth and velocity). This data is essential for clarifying and reconstructing the entire movement process of debris flows (Tecca et al., 2003; Suwa et al., 2009; Hürlimann et al., 2019).

Existing monitoring methods mainly involve installing instruments in debris flow channels to monitor hydrological parameters, such as water flow and water level, a variety of instruments, including infrasound sensors (Marchetti et al., 2019), LiDAR (Aaron et al., 2023), fiber optic sensors (Huang et al., 2012; Schenato and Pasuto, 2021), pressure sensors (Berti et al., 2000; Kean et al., 2012), and stress sensors (McArdell et al., 2007; McCoy et al., 2010; Nagl and Hübl, 2017), are increasingly utilized to capture a wide array of parameters. However, existing monitoring methods face challenges when it comes to collecting comprehensive data throughout the entire debris flow process. They require accurate identification of debris flows and the prior installation of monitoring instruments, as well as ensuring that these instruments remain intact during the debris flow. The sudden occurrence and violent impact of debris flows can damage nearby monitoring equipment and make data collection difficult. In addition, some existing methods for monitoring debris flows are limited to collecting data from

a specific cross-section rather than providing continuous data for the entire debris flow process.

In order to gain a more comprehensive understanding of the entire debris flow process and to collect more accurate and comprehensive data, it is essential to improve the monitoring capabilities for debris flows. There is an urgent need to develop new monitoring methods. Environmental seismology have been applied to monitor various geological events, including landslides (Li et al., 2017; Fuchs et al., 2018), rockfalls (Deparis et al., 2008; Vilajosana et al., 2008), avalanches (Schneider et al., 2010; Van Herwijnen and Schweizer, 2011), as well as debris flow (Arattano, 1999; Burtin et al., 2009; Schimmel and Hübl, 2016; Walter et al., 2017; Lai et al., 2018). The main benefits of environmental seismology are long-distance monitoring capabilities and detailed event dynamics (Arattano and Marchi, 2008; Hübl et al., 2013; Kogelnig et al., 2014). Belli et al. (2022) found that physical parameters (front velocity, maximum flow depth and density) of debris flows correlate positively with seismic signal amplitudes. Seismic monitoring can capture detailed event evolution, vital for analyzing debris flow characteristics and issuing warnings. Walter et al. (2017) successfully detected a debris flow half an hour before it reached a critical point, while Lai et al. (2018) proposed a method for calculating flow velocity and distance from seismic signal characteristics. Farin et al. (2019) introduced a model for estimating parameters related to debris flow dynamics, and Andrade et al. (2022) found a linear relationship between seismic signal amplitude and debris flow rate. However, high-frequency seismic signals from debris flows are challenging to detect due to their rapid attenuation and short propagation distances. These signals are often only recorded by close-range instruments (Zhang, 2021a, b). Unlike landslides, debris flows lack significant low-frequency features in seismic signals, making remote monitoring impractical. Understanding debris flow seismic signals and their source processes is still limited, but near-field seismic monitoring offers more detailed insights, enhancing event analysis. Therefore, near-field monitoring is the preferred method. Current research on debris flows focuses on

the timing, localization, parameter development, and detection of events with the aim of analyzing the entire debris flow process and providing references for debris flow hazard mitigation and early warning systems (Schimmel and Hübl, 2016; Lai et al., 2018; Beason et al., 2021; Andrade et al., 2022; Schimmel et al., 2022). The generation of debris flow seismic signals is closely related to the forces acting on the riverbed by the debris flow. Existing physical models of debris flow seismic sources are mainly derived from the theory of river transport and the theory of particle impact on the bed, and are closely related to the base forces acting on the riverbed (Tsai et al., 2012; Burtin et al., 2014; Farin et al., 2019; Zhang et al., 2021). However, since the particle impact on the riverbed during debris flow movement is extremely complex, there is currently no universally applicable debris flow seismic source model. Lai et al. (2018) suggested that high-frequency seismic signals from debris flows are closely related to the area of the head zone, the particle size contained in the debris flow, and the average flow velocity of the head zone. However, this model also assumes vertical particle impacts on the ground, neglecting the influence of channel shape and topographic variations on the particle impact angle. Kean et al. (2015) found that the sediment cover on the debris flow bed strongly suppresses ground vibrations. Belli et al. (2025) proposed that, in addition to particle collisions, turbulence also radiates seismic waves within the debris flow.

Although the debris flow seismic source model is not yet fully understood, experimental results from Allstadt et al. (2020) demonstrated that high-frequency seismic signals from debris flows can reflect overall movement characteristics, such as flow depth, gravity, density, momentum, and kinetic energy. The seismic signals generated during the debris flow process contain rich information about debris flow parameters (e.g., flow depth, particle size, flow velocity). Therefore, using seismic signals to reconstruct the debris flow process is a reliable method.

This study is based on the characteristics of debris flows in the Wenchuan region of China and uses a near-field debris flow observation system consisting of seismic

instruments, rain gauges, and infrared cameras. We collected data on three debris flows that occurred in Wenchuan on August 19, 2022. The data collected during these debris flows were then analyzed. First, we investigated the time-frequency characteristics of the seismic signals of the Wenchuan debris flows by short-time Fourier transform (STFT) and power spectral density (PSD). We also used the cross-correlation algorithm to compute the average velocity of debris flow. Subsequently, relevant motion parameters of the debris flow process were extracted from the seismic signals and combined with video and field investigation data to reconstruct the entire debris flow process.

2 Study site and field observation system

2.1 Study area

The study area is located in Wenchuan County, Sichuan Province, China (Fig. 1), characterized by north-northeast trending mountains divided by the Minjiang River and its tributaries. This region, formed by tectonic uplift and river erosion, features undulating terrain, ravines, and steep slopes. River gradients range from 5° to 30°, while hillslope gradients range from 25° to 50°. The climate is humid, with annual rainfall between 800-1200 mm (Guo et al., 2016). The area experiences frequent seismic activity, and signs of the May 12, 2008 Wenchuan Earthquake are still evident, with loose rocks and soils providing abundant sediment for debris flows (Zhang et al., 2023). This study focuses on the Er and Fotangba Gullies in the Minjiang River Basin, which has experienced numerous debris flow events in recent years, yearly frequency ranges from 0.17 to 2.67, threatening nearby villages, roads, and hydropower stations (Guo et al. (2016)). Notable incidents include 17 documented events by Guo et al. (2016), as well as specific events like the debris flow in Er Gully on July 10, 2013 (Guo et al., 2016), in Fotangba on the same date (Cao et al., 2019), and another in Er Gully on July 5, 2016 (Cui et al., 2018).

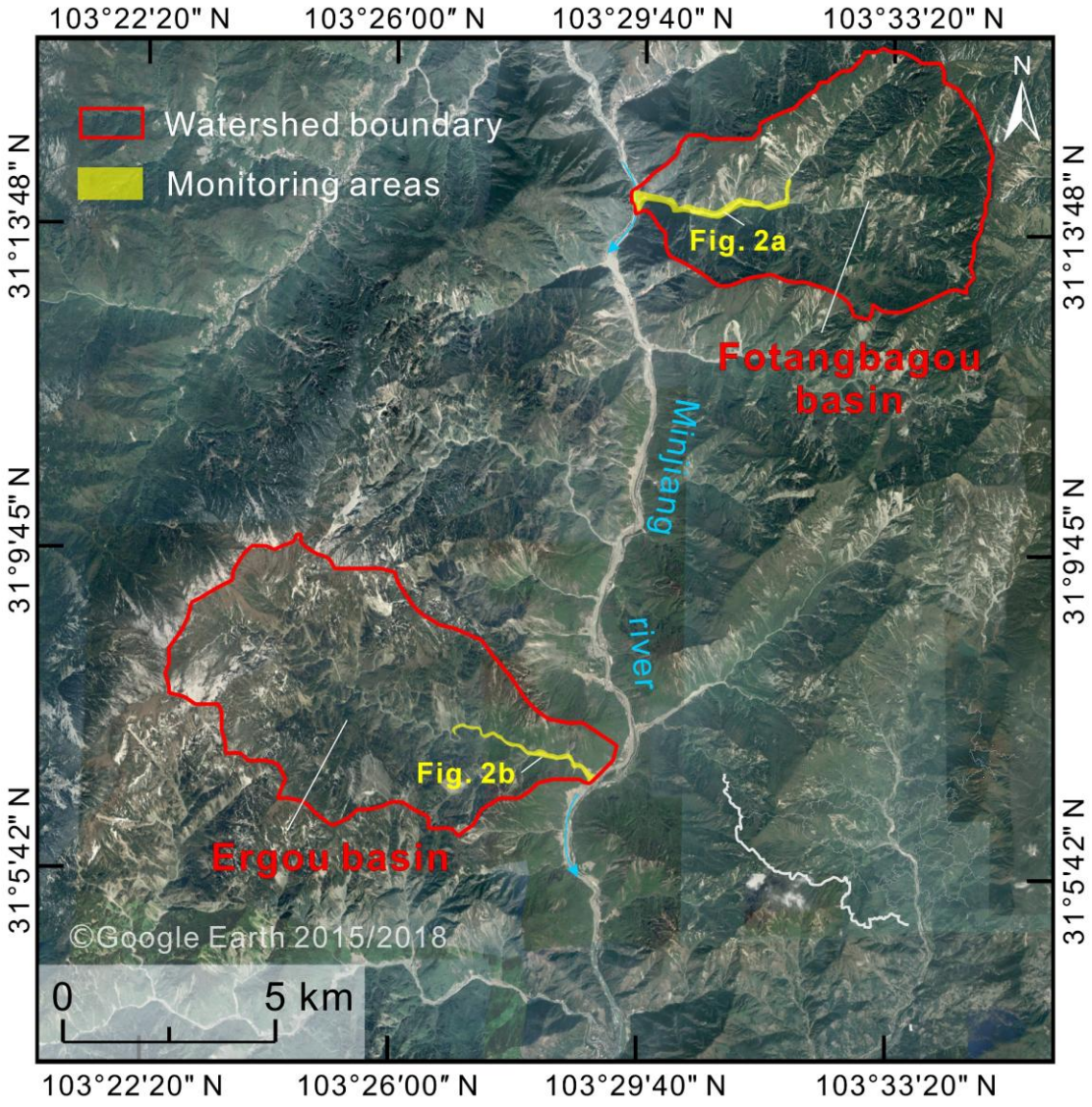

Fig. 1. The two study catchments, Er and Fotangba Gullies, on the Minjiang River, Wenchuan, Sichuan, China.

Er Gully drains an area of 39.4 km^2 and is about 6 km from the epicenter of the Wenchuan Earthquake; it ranges in altitude from 930 to 4120 m, has a channel length of about 12 km, an average slope of about 12° (Guo et al., 2016). The Fotangba Gully basin has an area of 33.6 km^2; it ranges in altitude from 1117 to 3462 m, has a channel length of about 9.78 km, with an average slope of 6.1°, and has bank slopes of 25° to 45° (Cao et al., 2019).

2.2 Observation systems

We have installed a near-field debris flow observation system at locations along the debris flow channels with unobstructed views. The system includes seismic

monitoring devices, infrared cameras, and rain gauges. The main function of the system is to comprehensively monitor the debris flow process through seismic signals and infrared camera images, while the rain gauges provide real-time precipitation data. The Fotangba Gully observation stations 1 and 2 are located 3,260 meters and 2,740 meters from the canyon entrance, respectively, while the Er Gully 0bservation stations 1 and 2 are located 4,130 meters and 3,670 meters from the entrance (Table 1, Fig. 2). The distance between the two monitoring stations in Fotangba Gully and Er Gully is 520 meters and 460 meters, respectively. Both monitoring stations are installed on rocky platforms on the left bank of the river. The two observation stations in Fotangba Gully are located approximately 20 meters and 15 meters from the centerline of the river. However, due to the lack of a network signal, real-time transmission of the recorded data via the Internet/GSM is not possible. The seismic monitoring devices operate at a sampling frequency of 100 Hz, and the infrared cameras are set to take images every 5 minutes. The specific parameters are listed in Table 1.

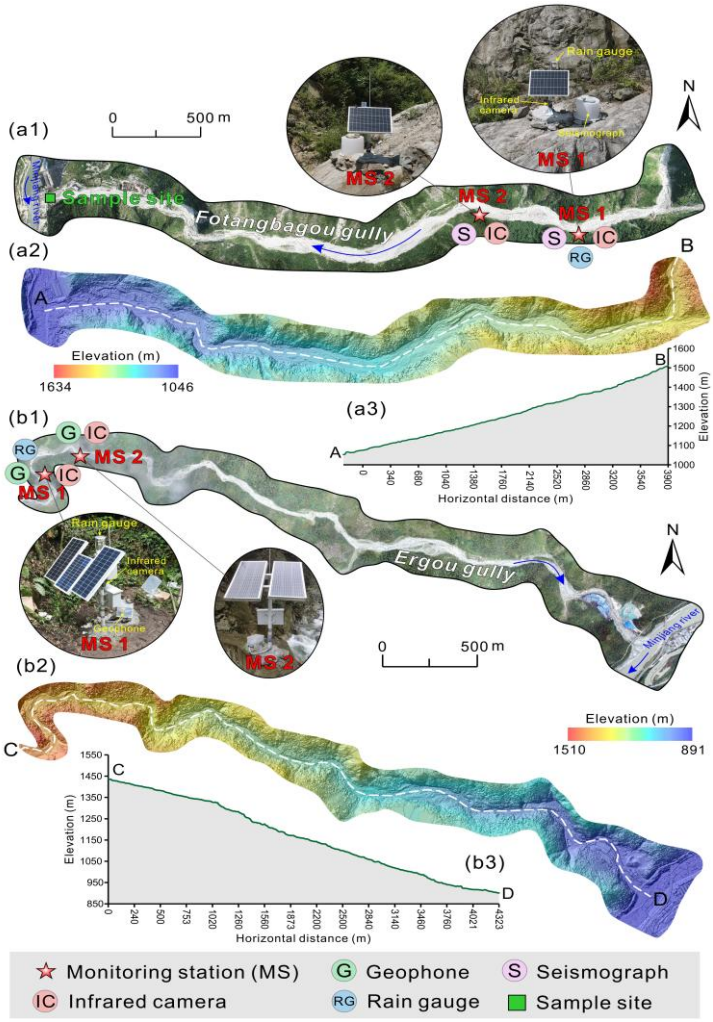

208

209 **Fig. 2.** Schematic overview of observation network layout in the two study catchments.

210 (a) Fotangba Gully: (a1) drone aerial photography, (a2) Digital Terrain Model map, (a3)

211 longitudinal profile; (b) Er Gully: (b1) drone aerial photography, (b2) Digital Terrain

212 Model map, (b3) longitudinal profile. See Fig. 1 for Gully locations.

213 **Table 1** Instrument parameters for observation stations in the two study catchments.

Equipment	Instrument parameters	
	Fotangba Gully	Er Gully
Seismograph	Sampling rate 100 Hz Corner frequency not offered Channel: Three components Sensor type: Capacitive force balance pendulum Dynamic range: Greater than 140 dB Bandwidth: 10 s - 50 Hz Sensitivity: 2000 V/(m/s)	—

Geophone	—	Sampling rate 100 Hz Corner frequency of 4.5–150 Hz Type: Delta-Sigma 24 Bit Channels: Three components Dynamic range: 125db @ 100sps (128db @ 50sps) Noise level: 10nV/sqrt (Hz) Input impedance: 100kOhm
Instrument response	Voltage sensitivity:2000V • S/m Normalized coefficient: 98696 Zero point: z1=0.0+0.0i z2=0.0+0.0i Main Pole: p1=-0.444221-0.6565i p2=-0.444221+0.6565i p3=-222.110595-222.17759i p4=-222.110595+222.17759i	Logger: "Cube3ext", Gain: 16 (DATA-CUBE³ User Manual)
Rain gauge	Record once per hour with a resolution of 0.2 mm	
Infrared camera	1 shot every 5 minutes at 2592×1944, 1920×1080 dpi resolution during the day and at night	

3 Methodology

With the aim to investigate to get the evolution of debris flow, we have designed the seismic signal processing and interpretation flow, as shown in Fig. 2. The power spectral density, time-frequency spectrum and simplified signal of the debris flow seismic signals by the compensated seismic data record by in-situ monitoring network in Fig. 2. The infrared imagery, Manning formula velocity, and other post-event on-site investigations will be used to validate the debris flow evolution reconstructed from the seismic signals. To achieve this, we designed a research methodology, as shown in Fig. 3.

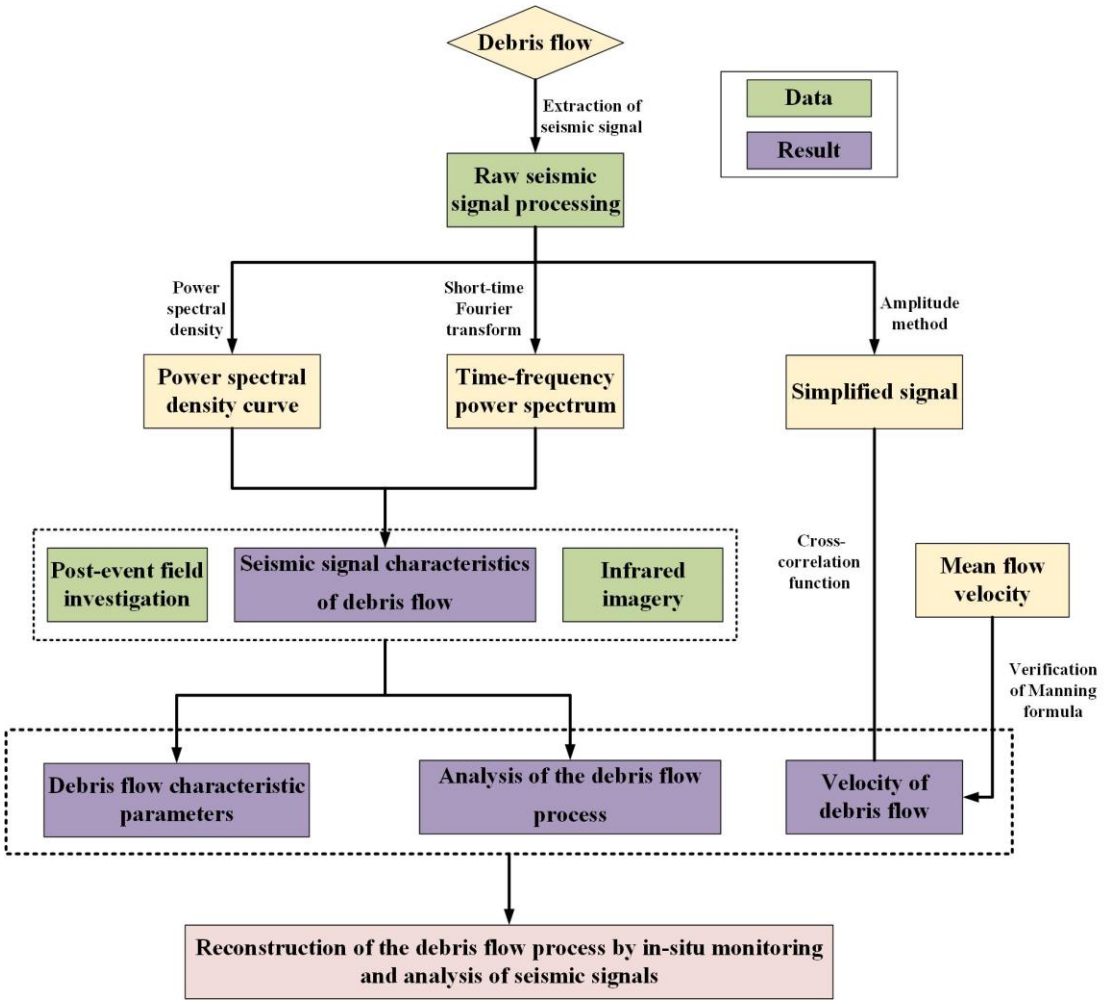

Fig. 3. Research methodology for processing and analysis of debris flow seismic signal.

Absorption attenuation compensation is first applied to the seismic signals of the debris flow to restore the different energy losses across frequencies. This helps to restore the original seismic excitation signals as far as possible so that the seismic signals more accurately reflect the changes in debris flow properties. The power spectral density (PSD) calculated from the compensated seismic signals is used to analyze the variations in the characteristic parameters of the debris flow based on the PSD model for debris flows proposed by Lai et al. (2018). The time-frequency spectrum is used to roughly analyze the overall changes in debris flow characteristics and to establish a preliminary framework for PSD analysis of these changes.

In addition, infrared images and on-site investigations are used to perform quality control of the debris flow development process reconstructed from the PSD analysis and to validate the accuracy of the analysis. Finally, a simplified signal, the absolute

value of the time domain amplitude (Arattano and Moia, 1999), is used to calculate the average flow velocity of the debris flow by cross-correlation, and the reliability of this result is verified using the Manning formula. Next, we will present some of our most important research methods in detail.

3.1 Power spectral density analysis

Tsai et al. (2012) developed a PSD model for sediment transport that links seismic signals with water turbulence, precipitation, and sediment transport in rivers. In their model, they considered the relationship between seismic signals and the transport of bedload in rivers. Tsai et al. (2012) adapted this model for debris flows by including absorption damping during the propagation process and established the PSD model for debris flows near the source shown in Eq. (1). This model links debris flow parameters such as length, particle size, width, velocity, and attenuation factors (due to absorption) as well as viscoelastic parameters during propagation with the seismic PSD of the debris flow.

$$PSD \approx 1.9 \cdot LWD^3 u^3 \cdot \frac{f^{3+5\xi}}{v_c^5 r_0} e^{-\frac{8.8 f^{1+\xi} r_0}{v_c Q}}, \quad (1)$$

where W is width of the channel, D represents the 94th centile of the grain size distribution, u represents debris flow velocity, f is frequency, v_c is Rayleigh wave phase velocity at 1 Hz, r_0 is distance between the monitoring station and channel, L is effective length of $L=r_0$, $\xi=0.4$ is a parameter related to how strongly seismic velocities increase with depth at the site, and Q is an attenuation factor (Tsai et al., 2012; Lai et al., 2018).

Debris flow seismic Power spectral density calculated by Eq. (2), which means the power per frequency for different frequencies in a specific period (Yan et al., 2020, 2022, 2023), and allows debris flow evolution to be analyzed from the seismic signal. The power of full band seismic is calculated by the short-time Fourier transform (STFT, Eq. 3), allowing getting the frequency domain characteristics of the signal versus time, which can help us to get the PSD changes versus the time.

$$PSD_{f_{\min}\sim f_{\max}}(t)=\frac{1}{(f_{\max}-f_{\min})}\times\sum_{f=f_{\min}}^{f_{\max}}X(t,f), \tag{2}$$

$$X(t,f)=\sum_{-\infty}^{\infty}x(m)W(t-m)e^{-j2\pi fm} \tag{3}$$

where f is the angular frequency, $f_{\min}$ and $f_{\max}$ represent minimum frequency and maximum frequency, respectively, t is time for the seismic signal, $X(t,f)$ represents the spectrogram based on STFT (Yan et al., 2017). x are time domain signals, W is the window function, m is the start time of the window function, e is a natural constant, t is time, and j is the imaginary number (Yan et al., 2021). A Hanning window length of 2056 and a time length of 20.56 s correspondingly is used. A built-in function "spectrogram" of MATLAB is used to achieve STFT directly from the software manual. The sampling rate is 100 Hz, so we choose 1 Hz and 50 Hz (i.e., a half of 100 Hz) as $f_{\min}$ and $f_{\max}$.

3.2 Absorption attenuation compensation

During the actual propagation of seismic waves through geological layers, scattering and absorption attenuation effects occur, which means that the phase velocity and group velocity are different and the amplitude of the seismic waves is subject to varying degrees of attenuation. This phenomenon has been well documented and studied in many related works (Futterman, 1962; Strick, 1967). In this study, we use the constant Q model (Kjartansson, 1979) to describe the absorption attenuation in the actual geological layers, and we have established a 1D plane wave amplitude attenuation equation for linear viscoelastic media (Eq. 4) to approximate the energy loss of seismic signals from debris flows during propagation. From this equation, it can be deduced that the amplitude of seismic waves is exponentially negatively correlated with both the propagation time and the frequency. In other words, as the propagation distance increases and the frequency rises, the amplitude of the seismic waves decreases significantly. This also explains why seismic signals from debris flows generally have lower frequencies when measured from greater distances.

$$h(t,f)=e^{-\frac{\pi ft}{Q}\left|\frac{\omega_0}{\omega}\right|^{\frac{2}{\pi}\arctan\left(\frac{1}{2Q}\right)}}, \quad (4)$$

where f is the frequency of the seismic signal, t is the spreading time (i.e., 0.02 s and 0.05 s) which is equal to distance r_0 between the monitoring station and channel divided by Rayleigh wave velocity v_c in Eq. (1), Q represents attenuation factor quantitatively depicting the absorption attenuation, and ω_0 and ω are reference angular velocity at 1 Hz (ω_0=2π) and angular velocities, respectively.

Direct use of Eq. (4) to compensate for absorption attenuation results in significant attenuation in the high-frequency range, leading to a lower signal-to-noise ratio (SNR) and an excessively large amplitude compensation factor. This can cause the compensated amplitude to become too large and the SNR to be extremely low (Wang, 2002). In this study, we will use the gain control method proposed by Wang (2002) (Eq. 5) to maintain the stability of the high-frequency range. This method aims to improve the energy of the high-frequency range while keeping the overall SNR of the entire frequency band relatively controlled.

$$\Gamma(t,f)=\frac{h(t,f)+\sigma^2}{h^2(t,f)+\sigma^2}, \quad (5)$$

where σ is a constant named stability control factor, whose value comes from a numerical experiment., with a σ^2 value of 0.02 used here.

After applying absorption damping compensation according to Eq. (5), not all absorption damping terms in Eq. (1) are completely compensated. However, the partial compensation of absorption damping allows the PSD and the time-frequency characteristics of the seismic signal to reflect the changes in the characteristic parameters of the debris flow more accurately. This allows the PSD of the seismic signal of the debris flow obtained using Eq. (2) to be analyzed more effectively using Eq. (1).

3.3 Cross-correlation function and Manning formula

Arattano and Marchi (2005) found that the velocity values calculated using cross-correlation were close to the measured velocity values. In the context of debris flows,

the average flow velocity between observation stations can be obtained by dividing the distance between the stations by the signal time delay. This method has been used to objectively calculate the mean velocity of debris flows (Coviello et al., 2015):

$$[x_K] = [x_0, x_1, x_2, \ldots, x_{M-1}] \tag{6}$$

$$[y_K] = [y_0, y_1, y_2, \ldots, y_{M-1}] \tag{7}$$

$$\phi_{yx}(\tau) = \sum_{t=0}^{M-1} x_t y_{t+\tau} \ , \tag{8}$$

where y from station 2 is another signal of time domain for the same event as x from station 1, t and K which are absolute sampling time series from 0 to M-1, ϕ represent cross-correlation function. When t exceeds M-τ-1 and is less than 0, x_t and $y_{t+\tau}$ is equal to 0.

The Manning formula (Eq. 9) is used to calculate the peak flow velocity of a debris flow passing through a section, based on characteristic terrain parameters of the section (Yu and Lim, 2003; Cui et al., 2013; Guo et al., 2016). Here, the velocity calculated using the Manning formula is compared with that from the cross-correlation method, to verify the relative accuracy of the cross-correlation algorithm:

$$v = \frac{1}{n} J^{\frac{1}{2}} R^{\frac{2}{3}} \tag{9}$$

where v represents debris flow velocity, n represents the roughness coefficient of the channel, J is the slope ratio of the section, and R is the hydraulic radius of the section.

In Eq. (9), n is calculated using Eq. (10) (Smart, 1999):

$$n = \frac{d_{50}^{\frac{1}{6}}}{6.7\sqrt{g}} \tag{10}$$

where d_{50} represents median particle size, and g represents the acceleration due to gravity.

4 Results and analysis

4.1 Characteristics of the debris flow seismic signal

4.1.1 Debris flow seismic and rainfall data

Based on the instrument response data in Table 1, the original seismic data was corrected for the instrument response and converted to velocity (m/s). Through a joint analysis of the seismic signals recorded by the observation system on August 19, 2022, and precipitation data, we were able to determine that two debris flows occurred in Fotangba and one in Er Gully. All three debris flows were likely triggered by precipitation. As shown in Fig. 4, significant amplitude increases and fluctuations in the seismic signals were observed during the debris flows. By analyzing the wavefield characteristics of the debris flows, we were able to determine the approximate times of all three events. The rainfall record for Fotangba Gully shows hourly rainfall of 6.4 mm and 14.2 mm before the first and second debris flows, respectively (Fig. 4e). In Er Gully, the hourly rainfall before the debris flow was 3.8 mm (Fig. 4f). Analysis indicates precipitation occurred before the three debris flows. Additionally, the rainfall data can be linked to the initiation time of the flows and significant changes in seismic signals. The two debris flows in Fotangba Gully coincided with the maximum hourly rainfall on the day of the events (second highest and highest) within a 24-hour period, while the Er Gully debris flow did not coincide with a maximum. However, the cumulative rainfall before the Er Gully debris flow reached 15 mm, greater than the cumulative rainfall for the first debris flow in Fotangba Gully. Therefore, rainfall is considered the triggering factor for debris flow initiation in both gullies.

The seismic amplitude of the three debris flow events showed a characteristic rapid increase followed by a gradual decline. However, the amplitude values and variation characteristics differed significantly. The seismic amplitude and duration of the second debris flow event in Fotangba Gully were both greater than those of the first event. The signal at measuring station 1 showed more pronounced changes during both debris flows than during periods when no debris flows occurred. We selected the seismic signals from the same time period on the day prior to the debris flow event as the background noise, and calculated the ratio of the debris flow signal power to the noise

power as the signal-to-noise ratio (SNR) (Fu et al., 2020). In terms of signal-to-noise ratio (SNR), the SNR for the first debris flow in Fotangba Gully was 20.66 dB and 7.96 dB, while for the second debris flow it was 19.60 dB and 15.80 dB. Similarly, at measuring station 2 in Er Gully, the amplitude and fluctuations of the seismic signals were higher than at station 1, with SNR values of 20.47 dB and 17.62 dB, respectively. For the same debris flow, the signals recorded by the two measuring stations showed considerable differences, which could be due to different sensor placement conditions and the degree of signal attenuation during propagation. In addition, differences in the flow dynamics of the debris flows at different stations probably also contributed to these deviations. When analyzing the seismic signal waveform, I found clear differences in the signal peak characteristics between different measurement points within the same channel. For example, at measurement point 1 in Fotangba Gully, the largest signal peak occurred during the second debris flow in the initial phase, with the subsequent peaks gradually decreasing. In contrast, the signal peaks recorded at measurement point 2 were similar in magnitude, and the number of peaks also differed between the two measurement points. A similar pattern was observed at measurement point 2 in Er Gully, where the largest peak occurred at the beginning of the event and the subsequent peaks gradually decreased. Several peaks of similar magnitude were observed at measurement point 1. These striking differences in signal characteristics at different measurement points within the same channel indicate that the dynamic parameters of the debris flow changed during its development.

Based on the above analysis, it was determined that the flow dynamics of debris flows recorded at different measuring stations can vary. In addition, the geological characteristics near the different stations differ, which prevents a direct comparison of the amplitude values between the two measurement points within the same channel. Therefore, our subsequent comparisons focus primarily on analyzing the development of debris flows over different time periods at a single station, while comparisons between different stations are mainly used to analyze the occurrence times of the debris

flows. Given the larger extent, longer duration, and lower curvature of the second debris flow in Fotangba Gully, as well as the better quality of the infrared images, we will use the second debris flow in Fotangba Gully as a case study in our future research to illustrate our analysis process.

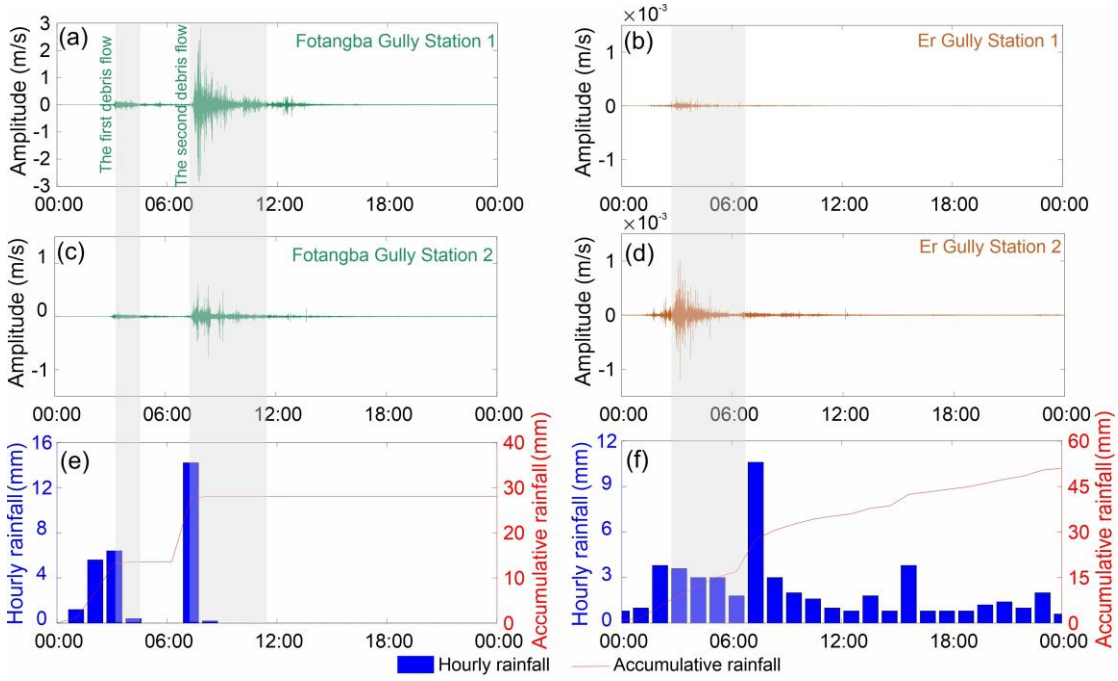

Fig. 4. Raw seismic signals and rainfall data. (a) and (c) represent monitoring station 1 and station 2 in the Fotangba Gully; (b) and (d) represent monitoring station 1 and station 2 in the Er Gully; (e) Rainfall at Fotangba Gully; (f) Rainfall at Er Gully.

4.1.2 Debris flow seismic energy recovery and time-frequency

We applied Eq. (4) and (5) to compensate for the maximum possible energy loss during the propagation of debris flow seismic signals. These signals were recorded along the river channel. As the debris flow travels through the channel, it generates vibration signals that propagate to the observation stations and are recorded by sensors. This seismic signal is a superposition of the vibration signals generated by the entire debris flow, characterized as a "line source." To accurately reproduce the energy of this "line source" seismic signal, it is essential to precisely determine the propagation paths of individual "sources." However, due to factors such as river channel morphology and surface velocity variations, this information is challenging to ascertain accurately. To

simplify the compensation process, we considered the area within 50 meters upstream and downstream of the monitoring station as the primary sources of the seismic signals recorded at the station. We calculated the geometric mean of seismic wave propagation times from the center of this 50-meter river channel to the monitoring station at 0.5-meter intervals, using this geometric mean as the seismic wave propagation time for energy compensation. Another important parameter is the velocity and amplification factor (σ^2) of the 1 Hz Rayleigh surface wave, which is influenced by the geological conditions near the monitoring station. Since we performed near-field observations, we neglected velocity variations near the station and assumed that the velocity of the 1 Hz Rayleigh surface wave remains constant. This assumption simplifies the geometric mean of the transit times to the geometric mean distance of this flux section relative to the observation point. The amplification factor (σ^2), ensuring numerical stability, was determined through numerical experiments. The principle of these experiments was to expand the compensation frequency range as much as possible while maintaining a high signal-to-noise ratio for the debris flow signal.

Under the help of near-surface velocities investigations in using petroleum seismic technique (Liu et al., 2013), we analysis the surface conditions near the second debris flow event in Fotangba Gully and determine the Q values and reference velocities for two specific locations in Fotangba Gully. The Q values were found to be 4 and 2.4, with corresponding Rayleigh wave velocities of 800 m/s and 500 m/s at a frequency of 1 Hz. We calculated the geometric mean travel times for these two locations to be 0.02 seconds and 0.04 seconds, respectively. After numerous numerical experiments, we set the gain control factors for both locations to 0.02.

From the compensation spectrum curve, the high-frequency components have been significantly restored, and both sites show similar improvements in their spectrum curves (Fig. 5). The time domain curve indicates that the characteristic changes at site 2 after compensation further enhance its similarity to site 1, with these changes being more pronounced. In terms of effectiveness, the compensation has proven to be quite

effective, as it mitigates the absorption attenuation of the debris flow seismic signals to some extent. Therefore, in the following sections, we will use the compensated seismic signals for further analysis of the second debris flow event at Fotangba Gully.

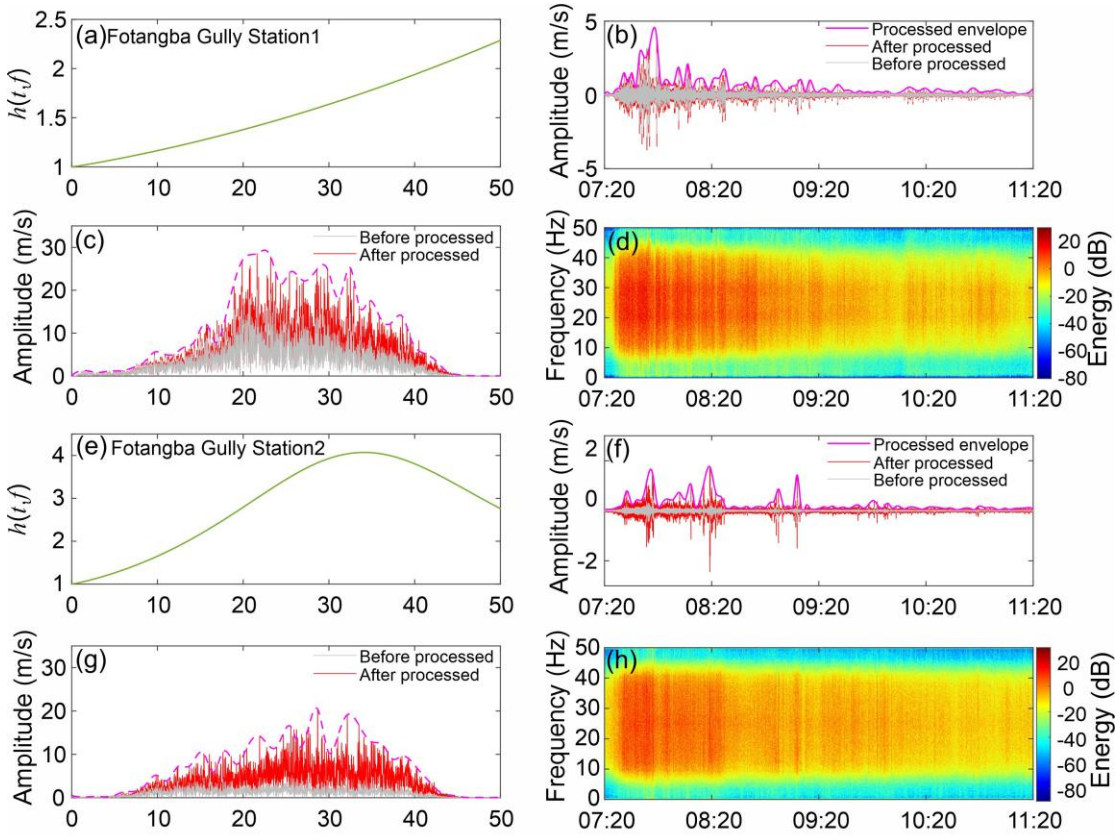

Fig. 5. Restored seismic signal for the second debris flow in Fotangba Gully. (a) Compensation function curve for monitoring station 1; (b) Time domain signal at monitoring station 1; (c) Frequency domain signal at monitoring station 1; (d) Restored spectrogram for monitoring station 1; (e) Compensation function curve for monitoring station 2; (f) Time domain signal at monitoring station 2; (g) Frequency domain signal at monitoring station 2; (h) Restored spectrogram for monitoring station 2. The red dashed lines in (c) and (g) are envelopes that represent peak amplitudes after processing.

At monitoring point 1, the signal amplitude and frequency range rapidly increased when the debris flow occurred. The frequency range primarily concentrated between 8 Hz and 43 Hz. During the debris flow event, the energy initially concentrated and then gradually decreased, with a range between -120 dB and -60 dB. The data from monitoring point 2 was essentially consistent with that from monitoring point 1,

recording the debris flow starting at 7:26 AM, with a peak amplitude observed around 7:45 AM, followed by a gradual decline. However, there were minor differences in the frequency bandwidth at monitoring point 2, which concentrated between 10 Hz and 40 Hz. The energy variation trend and range were almost the same as those at monitoring point 1. Throughout the entire debris flow event, the observed peak frequencies at the two monitoring points were 21.6 Hz and 28.6 Hz, respectively. The frequency evolution between the two points indicates an increase in the peak frequency, which may be related to changes in particle impacts and scale. Factors such as rock falls and channel erosion might also influence the peak frequency. To reflect the surge wave characteristics, we used the upper envelope of the signal waveform (Fig. 5b and 5f). The surge waves corresponded with the wave characteristics of the debris flow, and the number of surges matched the number of waves. The flow depth between the surge waves was significantly discontinuous, with a sudden increase in flow depth from one surge to the next, similar to the characteristics of the surge flow. Monitoring point 1 observed about 8 significant surge waves, while monitoring point 2 recorded 7. Additionally, we noticed that monitoring point 2 recorded two significant surge waves around 9:00 AM, while monitoring point 1 did not observe any significant surges at the same time. This indicates that the flow dynamics of the debris flow between the two monitoring points along the river channel have changed, possibly due to variations in channel topography and the solid-phase content of the debris flow.

Overall, the trends in the time-domain and time-frequency spectra at the two monitoring points are similar, exhibiting rapid increases followed by gradual declines, consistent with the overall movement of the debris flow. However, Monitoring Point 1 recorded higher average amplitudes, wider frequency bands, and stronger energy. This may be attributed to the shorter distance between Monitoring Point 1 and the Gully, resulting in less energy loss during the propagation of seismic signals from the debris flow. Additionally, varying geological conditions may also contribute to the differences in seismic signal attenuation between the two monitoring points.

475 **4.2 Post-event field investigation**

476 Field investigations and UAV surveys at Fotangba Gully began three days after the
477 debris flow events, and local villagers confirmed that the accumulation fans had not
478 been disturbed. UAV aerial images of the accumulation fan at the Gully mouth, along
479 with close-ups of surface conditions, are shown in Fig. 6a to 6c. Field measurements
480 indicate that the fan thickness at location ① is about 1.2 m, with a thin layer (1 – 2 mm)
481 of clay covering the surface in some areas (Fig. 6c). Some rocks larger than 1 m in
482 diameter (Fig. 6b and 6c) suggest that the debris flow had a relatively high carrying
483 capacity. Larger rocks are found at the bottom of the alluvial fan (Fig. 6b), while smaller
484 rocks are located at the front (Fig. 6c), indicating that the carrying capacity of the debris
485 flow decreases sharply after being released from the channel constraints as the cross-
486 sectional area increases.

487 A sediment sample weighing about 4.7 kg was collected from the accumulation
488 fans in Fotangba Gully to estimate the particle size distribution of the debris flow, taken
489 from location ① in Fig. 6a. Grain size analysis was performed using sieving and a
490 Malvern particle sizer. Due to the lack of several sample analyses in this study, more
491 analyses should be conducted for better variability estimation. We also neglected to
492 record the portion of materials above the maximum particle size shown in the
493 granulometric curve, which should be addressed in future research. The results indicate
494 that clay particles (size < 0.005 mm) made up only 0.041% of the total sample weight
495 (Fig. 6d), consistent with field observations. The low cohesive sediment content in the
496 accumulation fan sample may result from removal by post-event processes, such as the
497 flushing action of the Minjiang River or human clearance. The particle size distribution
498 shows that 94% of the sample particles are 0.018 m, denoted as D in Eq. (1). In the next
499 section, we will use D as a basis for analyzing the PSD curve features of the debris flow.
500 Field investigations confirmed the occurrence of debris flows and provided data on the
501 maximum size of the boulders and the grain size distribution. These findings provide
502 valuable information for the subsequent reconstruction of the debris flow process and

the analysis of its parameters.

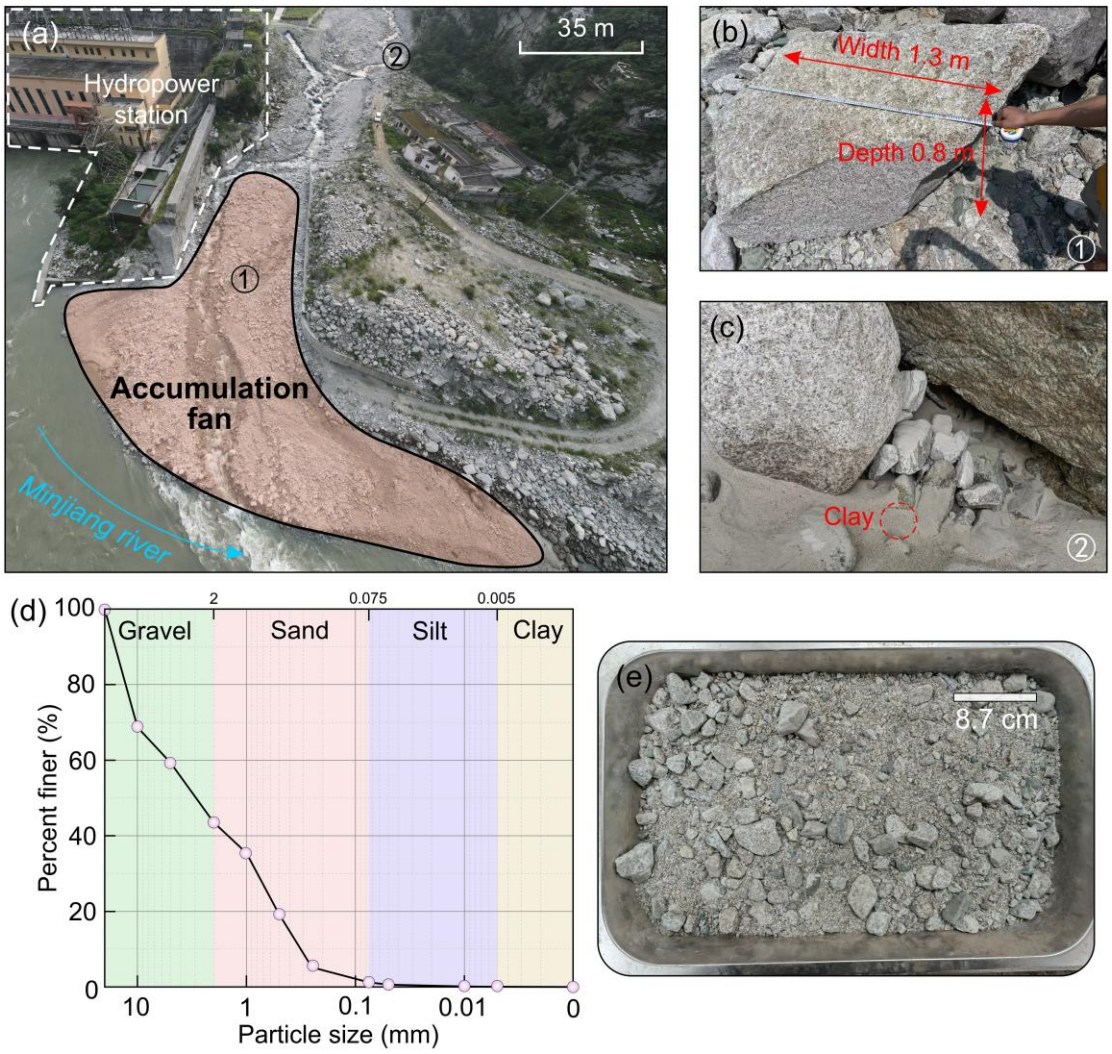

Fig. 6. Post-event field survey of accumulation fans in Fotangba Gully. (a) Aerial view of the Fotangba Gully fan; (b) Largest particle on the Fotangba Gully fan, marked ① in image (a); (c) Thin layer of clay covering the accumulation surface in Fotangba Gully, marked as ② in image (a); (d) Particle size distribution for Fotangba Gully sediment samples; (e) Fotangba Gully sediment sample. Clay has not been marked in the subplot (d) because the particles with grain size less than 0.005 mm account for 0.041% of the total weight of the sample.

4.3 Reconstruction of the debris flow process and analysis of characteristic parameters

4.3.1 Debris flow breaking time picked by seismic signals

By analyzing the seismic signal characteristics of debris flows in Section 4.1, we selected seismic data from observation point 1 at the Fotangba Gully and observation point 2 at the Er Gully to reconstruct the event times of the debris flows. We estimated the start, duration, and end of the debris flow events by observing sudden changes in the amplitude and frequency spectrum of the seismic signals. As shown in Fig. 4 and Fig. 5, the seismic signal in the Fotangba Gully initially showed a sharp increase in amplitude and energy at 3:07 a.m. The signal then continued to rise, reaching its peak at 3:13 a.m. and gradually declining until it stabilized at 5:26 a.m. At approximately 7:25 a.m., the signal changed again, and at 7:42 a.m., the amplitude reached its second peak, stabilizing around 11:24 a.m. In Er Gully, the seismic signal began to change at around 2:44 a.m. and stabilized at around 4:49 a.m. Based on this, we have made a preliminary reconstruction of the timing of the debris flows. The results show that the first debris flow in Fotangba Gully began at 3:07 a.m., gradually intensified, and ended at 5:26 a.m., lasting about 2.5 hours. The second debris flow in Fotangba Gully began at 7:25 a.m., intensified, and began to slow down at 7:42 a.m., finally ending at around 11:24 a.m. and lasting approximately 4 hours. The debris flow in Er Gully began at 2:44 a.m., slowed down at 2:58 a.m., and ended around 4:49 a.m., lasting approximately 2 hours (Table 2).

Table 2 Starting and ending time of three debris flow events at Wenchuan, China (August 19, 2022), picked from the seismic signals.

	Fotangba Gully		Er Gully
	1st	2nd	
Starting	03:07 am	7:25 am	2:44 am
Ending	05:26 am	11:24 am	4:49 am

Building on a clear understanding of the temporal sequence of the debris flow, we further analyzed the development of the debris flow process by combining seismic signal data and image material.

4.3.2 debris flow processes analysis based on infrared imagery

Continuous analysis of infrared imagery of debris flow characteristics can validate the evolution processes indicated by seismic signals. However, the analysis is hindered by the low quality of the initial debris flow images captured at night with a limited visible range and low resolution from Fotangba Gully and Er Gully. Therefore, this study utilizes the infrared imagery collected of the second debris flow in Fotangba Gully during daytime.

During the debris flow event, we captured infrared images at 5-minute intervals from 7:39 to 8:04 (Fig. 7b to 7g). Due to blurriness from water droplets on the camera lens at Monitoring Point 2, we relied solely on the infrared camera at Monitoring Point 1. The images showed that at 7:39, the debris flow volume was low, and the channel had not yet been submerged. Most of the flow is concentrated in the right channel, with less flow in the left channel. By 7:44, the debris flow began to submerge Point A and erode the left bank at Point B. Water depth and left bank erosion peaked at 7:59, after which water depth started to decrease. Overall, the infrared images indicated a gradual increase in flow from 7:39 to 7:54, followed by a decrease.

Flow velocity peaked at 7:39 and then gradually decreased, remaining relatively stable in subsequent images. The maximum turbulence at Point C indicated the highest flow velocity, which then gradually declined. The vortices near Point A suggested higher flow velocities, while the fluid patterns upstream at Point C indicated slower speeds. The vortices near Point C may have been caused by excessive discharge from lower elevations. Notable surges were observed in Fig. 7b to 7e, particularly at 7:49 and 7:54, with significant debris flow surges. From 7:39 to 7:59, the debris flow volume gradually increased due to higher flow velocities, which eroded the sediments along the channel, enhancing solid-phase material content and flow volume. After 7:59, the reduced flow velocity led to weaker erosion and a gradual decrease in particle content, evolving into a "flood" state. The debris flow surges matched the small peaks observed in the seismic signals. The trends in particle content mirrored those of flow volume,

gradually increasing from 7:39 to 7:49, remaining high from 7:49 to 7:54, and significantly decreasing at 7:59 and 8:04.

Through the analysis of debris flow evolution, we found that flow volume gradually increased from 7:39 to 7:59, with flow velocity peaking at 7:39 before gradually decreasing and experiencing multiple surges. The image analysis largely matched the debris flow evolution reconstructed through seismic signals, and the corresponding image timestamps further confirmed the consistency between the characteristics of the Fotangba Gully seismic signals and the observations from the images, supporting the accuracy of reconstructing the second Fotangba Gully debris flow event through seismic signals. However, the peak times were not entirely consistent with the seismic data, possibly due to the 5-minute recording interval.

By combining seismic signal data with image analysis, we achieved an accurate reconstruction of the second debris flow event at Fotangba Gully based on its temporal progression and evolutionary characteristics. In the following sections, we will integrate these variables with the forward modeling results of the seismic power spectral density (PSD) generated by the debris flow. This will allow us to explore the effects of flow velocity and particle size distribution, thereby analyzing the changes in characteristic parameters during the debris flow motion process.

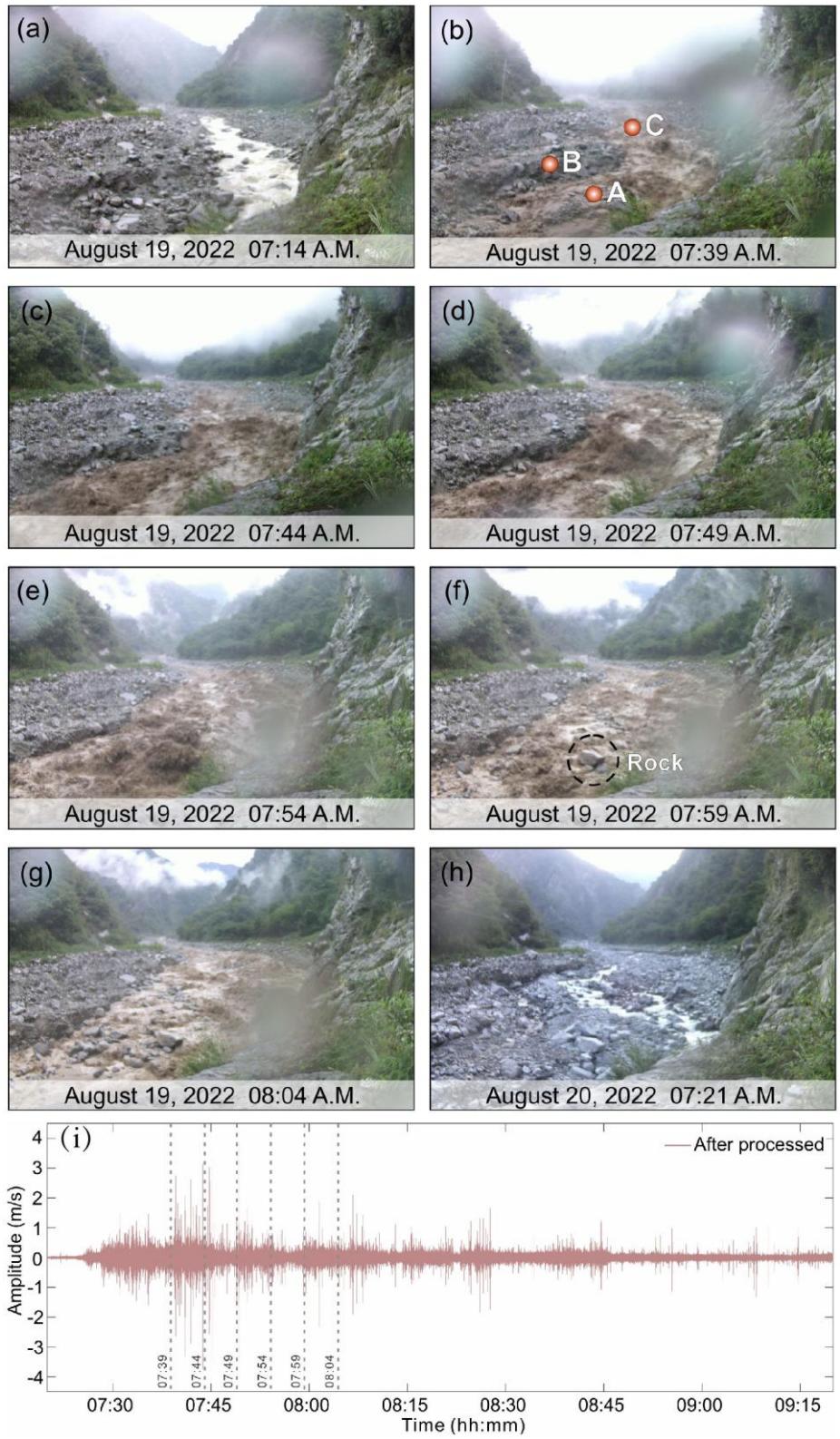

584

585 **Fig. 7.** Infrared camera images taken and the seismic signal recorded at monitoring
586 station 1 in Fotangba Gully during the second debris flow on the morning of August 19,
587 2022. Images were recorded every 5 minutes: (a) 7:14 frame (b) 7:39 frame; (c) 7:44

frame; (d) 7:49 frame; (e) 7:54 frame; (f) 7:59 frame; (g) 8:04 frame; (h) August 20, 2022, 8:04 Frame; (i) seismic signal recorded at the point.

4.3.3 Debris flow velocity analysis

In Section 4.3.1, we established the accuracy of the entire debris flow reconstruction process. However, some characteristic parameters of the debris flow process have not been quantitatively analyzed. This subsection will use seismic signal data to calculate the average flow velocity of the debris flow process. Cross-correlation functions can calculate the time delay between two measuring stations for debris flows, as shown in Eq. (8). The average flow velocity can be derived from the distance between neighboring observation stations and this time lag. Arattano et al. (2012), Comiti et al. (2014), and Schimmel et al. (2022) installed seismic instruments in different regions and found that the cross-correlation function can effectively calculate the debris flow velocity. In their studies, the measurement points were arranged along almost straight river channels, with the distance between the measurement points and the center of the channel being less than the straight-line distance between the measurement points. At the Fotangba Gully, the channel between points 1 and 2 is relatively flat and linear with a gradient of about 9°. The straight-line distance between these two points is 520 meters, which is greater than the 25 meters distance between the measuring points and the center of the channel. This arrangement of the instruments is similar to that in the studies mentioned above. In contrast, the river channel between the two measuring points in the Er Gully is convex (Fig. 2b) and has a gradient of around 16°. The distance between the two measuring points is approximately 460 meters, which is greater than the 200 meters straight-line distance between the two points. This instrument arrangement differs significantly from those used in previous studies. Therefore, our research mainly focuses on using the cross-correlation function to calculate the debris flow velocity at the Fotangba Gully.

The sampling rate for seismic signal monitoring is 100 Hz. The average amplitude for each second of seismic data is calculated using the amplitude method (Arattano,

1999), whereby 100 seismic signals are recorded within each second and their amplitudes are averaged. This method helps to smooth out high-frequency noise and provides a more stable representation of the amplitude of the seismic signal. Using simplified time domain signals processed with the seismic amplitude method, the φ_{yx} of the time domain signal for the second debris flow event in the Fotangba channel was calculated (Fig. 8a), with a time delay τ of 74 s corresponding to the maximum value of φ_{yx} for this event. The amplitude range for calculating flow velocity based on the cross-correlation function for the second debris flow event is shown in Fig. 8b. The distance between monitoring sections in the Fotangba channel is 520 m, resulting in an average velocity of 7.0 m/s for the second debris flow. To further validate the cross-correlation algorithm's applicability, we calculated average flow velocities of 3.0 m/s for the first debris flow event and 38.3 m/s for the Er Gully event using the same method (Table 3). The velocity for Er Gully was significantly higher than those for the two debris flow events in Fotangba and exceeded the flow velocities of 1-6 m/s observed by Cui et al. (2018) in the S1 section, indicating it may be inaccurate.

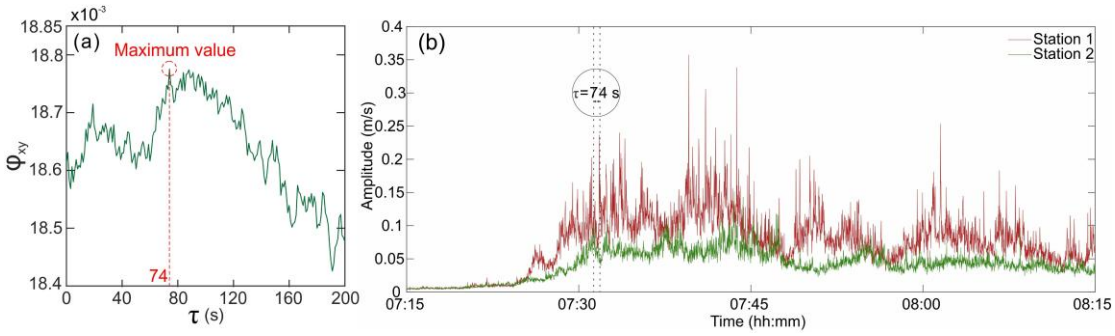

Fig. 8. The cross-correlation algorithm calculates the second debris flow in Fotangba Gully. (a) signal lag time τ between two observation stations; (b) Amplitude range of debris flow (vertical direction).

To verify the reliability of the velocity calculations derived from the cross-correlation function, the average velocity was also computed using the Manning formula (Yu and Lim, 2003; Cui et al., 2013; Guo et al., 2016). Channel parameters were obtained from the cross-sections at the observation stations (Fig. 9). The channel roughness coefficient *n* was set at 0.05 (Xu and Feng, 1979). The gradient

ratio *J* for the monitoring section was determined from the output of the UAV aerial survey's digital surface model (DSM). For monitoring station 1, the area and wet perimeters were 17.7 m² and 14.2 m, respectively. For the other cross-section, these values were 27.5 m² and 21.6 m. Consequently, the hydraulic radii *RR* for the two observation stations were 1.25 m and 1.27 m, respectively. The Manning formula calculation yielded a flow velocity of 7.921 m/s for the second debris flow event at Fotangba, which is in close agreement with the velocity of 7.027 m/s obtained through cross-correlation calculations. Additionally, the field investigation results in Section 4.2 revealed that the largest boulder displaced by the debris flow had a diameter of approximately 1.3 meters. Preliminary analysis through imagery suggests that the debris flow is of a dilute type. Reference to relevant literature on river transport indicates that a flow velocity of 7.027 m/s is capable of transporting boulders with a diameter of around 1.3 meters. Therefore, this suggests that the flow velocity obtained through the cross-correlation algorithm in this study is reliable.

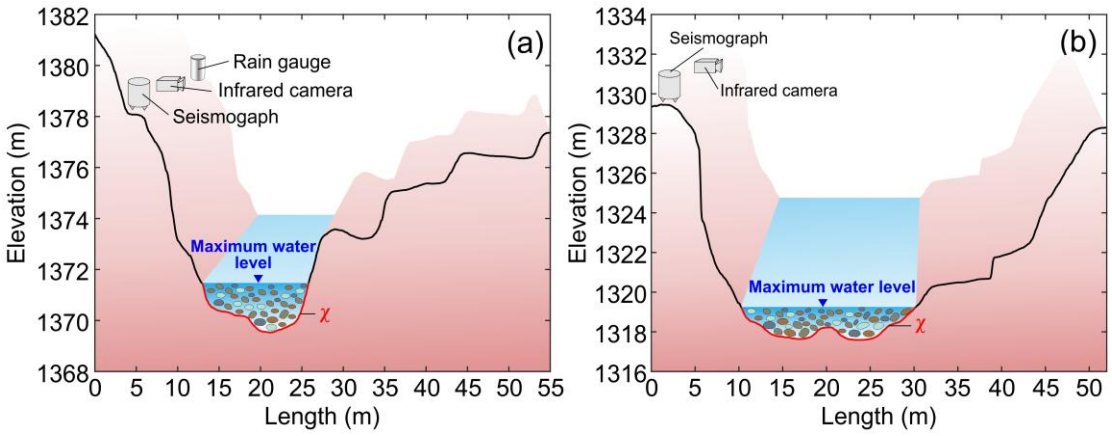

Fig. 9. Cross-sections of Fotangba Gully showing maximum water level used in calculation of mean velocity by the Manning formula. (a) Monitoring station 1; (b) Monitoring station 2.

Table 3 Results of maximum velocity calculations for Fotangba Gully and Er Gully debris flows.

Debris flow	Maximum velocity calculated using each method (m/s)	
	Cross-correlation	Manning formula

	algorithm	
First debris flow in Fotangba Gully	3.006	—
Second debris flow in Fotangba Gully	7.027	7.921
Debris flow in Er Gully	38.333	—

4.3.4 Analysis of changes in debris flow characteristic parameters by PSD

In Sections 4.2 and 4.3.3, the particle size distribution and average flow velocity of this debris flow were obtained, respectively. Based on this, the seismic power spectral density (PSD) is utilized to analyze the variations in the characteristic parameters of the debris flow. PSD curves for six time points, corresponding to their infrared images (Fig. 7b to 7h), were calculated using Eq. (1) (Fig. 10a). These curves show a clear decrease in maximum power energy from 7:39 to 8:04, with power energy initially increasing with frequency before decreasing. The peak frequency, which is the frequency corresponding to the maximum energy marked by black dots in Fig. 10a, increased slightly first and then a significant large increase and decrease, which flowed by slight decreases over time. Spectral width shows a feature of first broadening, which get the widest at 7:44, and then gradually narrows, but changes at different times are still relatively complex. We partitioned the frequency range into three parts for the analysis of PSD variation characteristics: low frequency (<15 Hz), medium frequency (15-30 Hz), and high frequency (>30 Hz). The PSD of high frequency decreased rapidly from 7:39 to 7:47, while a spike in low frequency occurred from 7:39 to 7:44, followed by a quick drop from 7:44 to 7:54. The frequency changes during the rest of the time were not significant.

The amplitude of PSD shows a gradually decreasing trend, reflecting that the flow velocity of debris flows as a whole shows a decreasing trend. D94 grain size, flow velocity, width and length of the channel only influence the PSD amplitude (Eq. 1), while r_0, v_c, and Q affect the shape of the PSD. The parameters, width and length of debris flow, which are positively correlated with flow velocity given the short duration

683 of the event, mainly characterize the flow volume, which determines the volume of
684 particle hitting the riverbed, and has a linear relationship with the PSD amplitude. We
685 assumed that D94 grain size is proportional to flow velocity, given that starting velocity
686 is proportional to the square of the particle size and the force maintaining the movement
687 of particles is much smaller. So, the amplitude is reckoned to be scaled to the sixth
688 power of the flow velocity (Eq. 1). Based on the above analysis, we can consider that
689 the PSD energy is mainly controlled by the flow velocity of the debris flow. The
690 amplitude of PSD showing a gradually decreasing trend, reflect that the flow velocity
691 of the debris flow is gradually decreasing, and the extent of the debris flow speed
692 reduction is gradually decreasing.

693 Propagation distance (r_0), Rayleigh wave phase velocity at 1HZ (v_c), and
694 attenuation factor (Q) determine the spectrum shape characteristics of PSD (Eq. 1). We
695 investigated the effect of these three parameters and linked the frequency features
696 variation and dynamic parameters of debris flow via a simple forward algorithm based
697 on Eq. 1. The key parameters were derived from the second debris flow at Fotangba
698 Gully: the D94 value is determined by the 94th centile of the grain size distribution; the
699 flow velocity of 7 m/s is obtained through cross-correlation calculation; the r_0, v_c, and
700 Q are set near the values during the seismic signal restoration. The results are shown in
701 Fig. 10b. The peak frequency of PSD shifts towards a higher frequency and a broader
702 band as r_0 decreases or a contrary alteration of v_c and Q.

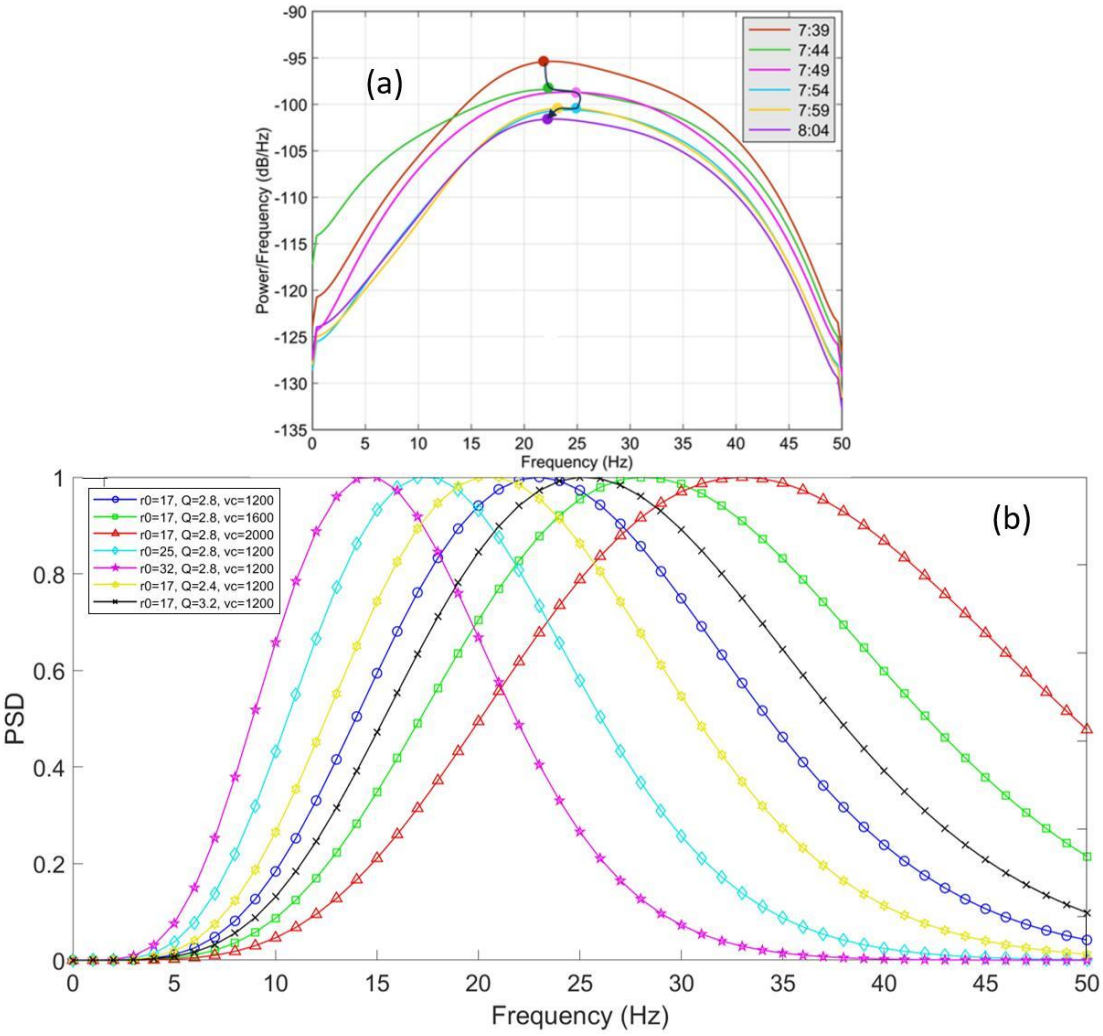

Fig. 10. Characteristic change of power spectral density (PSD). (a) Evolution of PSD during the second debris flow in Fotangba Gully on the morning of August 19, 2022, from 7:39 to 8:04; (b) Comparison of PSD for different r_0, Q, and v_c. The six dots in subplot (a) correspond to the PSD maximum at the six-time points from 7:39 to 8:04, and the black arrows indicate the time course of these six-time points.

In our study, the seismic signals generated by the vibrations of debris flow particles with the riverbed within a certain range around the sensors are superimposed and received. We assumed that the variation of v_c and Q near the channel mainly composed of debris flow deposition changes slightly. The seismic signals, generated by debris flow channel farther away from the sensor, travel much longer leading the seismic mainly dominated by low-frequency signals and with relatively low peak frequencies; whereas the seismic signal from the nearby channel is opposite, dominated by high-

716 frequency signals and with relatively high peak frequencies. Flow velocity, flow
717 volume, and particle content vary throughout the entire river channel. The seismic
718 signals received from the debris flow with a high velocity, massive volume, and rich
719 particle content primarily consist of low frequencies with lower peak frequencies.
720 Conversely, the signals are mainly high frequencies under the opposite conditions. The
721 low- and high-frequency energy shows a substantial enhancement from 7:44 to 7:49,
722 along with an alteration in the peak frequency toward a higher frequency, indicating an
723 increasing signal strength at different propagation distances. In contrast, low-frequency
724 energy decreases and high-frequency energy stays stable at 7:54, suggesting that the
725 seismic energy from distant sources weakens and from nearby sources remains steady.
726 The variation of grain concentration (flow volume and particle content) near the
727 channel affects the shape of PSD. An anomaly observed at 7:44 in low-frequency
728 energy is due to the upstream flow volume rising. As debris flow with high grain
729 concentration moves toward the sensors and flows downstream, the low-frequency
730 energy decreases and eventually recovers to a normal level.

731 We believed that the flow velocity decreases and grain concentration follows a
732 trend of increasing first and then dropping during the six key moments with a 5-minute
733 sampling interval from 7:39 to 8:04. The results are consistent with the findings from
734 infrared image analysis in Section 4.3.2, demonstrating that analyzing the evolution of
735 the debris flow using the time-frequency characteristics of seismic signals is feasible.

736 **5 Discussion**

737 **5.1 Characteristics and evolution of debris flow events**

738 This study successfully monitored three debris flows in Wenchuan, China, using a
739 seismic signal-based observation system. Given the quality and completeness of the
740 data collected, particular attention was paid to the second debris flow in Fotangba Gully.
741 By analyzing the seismic signal characteristics in combination with time-delayed
742 camera recordings and post-event investigations, the debris flow process and changes
743 in characteristic parameters were examined, leading to the reconstruction of the second

744 debris flow process in Fotangba Gully. The seismic signals of the three mudflow events
745 showed similar amplitude and time-frequency characteristics. However, differences in
746 the monitoring locations led to deviations in signal propagation and attenuation. By
747 applying compensation functions to partially restore the original seismic signals, signal
748 attenuation was minimized, allowing the movement of the debris flow to be mapped
749 more accurately. The seismic signal characteristics captured the entire course of the
750 debris flow process, and in combination with image analysis from time-lapse cameras,
751 the development of the debris flow could be derived more accurately. After determining
752 the entire movement sequence of the debris flow, characteristic parameters of the debris
753 flow were extracted from the seismic signals. These parameters were then verified by
754 field investigations, ensuring the accuracy of the reconstruction of the debris flow
755 process.

756 The average velocity of the second debris flow event at Fotangba Gully, calculated
757 using the cross-correlation function, was validated as reliable by the Manning formula.
758 However, using the same method, the flow velocity of the Er Gully debris flow was
759 calculated to be 38.3 m/s. Due to the damage observed in the Er Gully debris flow
760 images and at the site, we were unable to verify this result using the Manning formula.
761 Since this velocity exceeds the 1-6 m/s range found by Cui et al. (2018) for the Er Gully
762 debris flow, we infer that the flow velocity derived from the cross-correlation
763 calculation for this event is likely incorrect. Upon reviewing previous studies that used
764 the cross-correlation algorithm to calculate debris flow velocities, we found that the
765 channels between the two measurement stations in these studies were relatively straight
766 (with small curvature) (Arattano et al., 2012; Comiti et al., 2014; Schimmel et al., 2022).
767 By comparing the locations of the Er Gully and Fotangba Gully observation points, we
768 hypothesized that the significant curvature of the channel between the two observation
769 points in Er Gully may be a key factor. Therefore, directly using the cross-correlation
770 algorithm to calculate the flow velocity for debris flows in highly curved channels
771 between monitoring stations may not be reliable.

When selecting the analysis period for the power spectral density (PSD) curve, it is important to consider the characteristics of the seismic signals and select representative time points. It is also recommended to estimate both the flow velocity and the particle size, as these factors can significantly influence the PSD curve. By integrating detailed data from post-disaster investigations, dynamic parameters, and results from forward simulations, the reliability of seismic signal-based analysis of the development process of debris flows can be significantly improved.

5.2 Limitations and future works

Although this study successfully reconstructed the debris flow process, the reconstruction was based mainly on time and monitoring location cross-sections due to the limited and unsystematic monitoring instruments (which only included seismic monitoring devices and time-lapse cameras). It was unable to provide a detailed analysis of the debris flow process at all locations, as is possible with numerical simulations. However, by combining the seismic signal characteristics with the image analysis of the time-lapse cameras, we were able to gain a better understanding of the timing and duration of the debris flow and extract parameters such as flow velocity and particle size. These findings are valuable for understanding debris flow dynamics.

In this study, the seismic signals alone were not sufficient to fully reconstruct the debris flow process, which is why the image analysis from the cameras was also included. However, some problems arose with the use of infrared cameras. The cameras were unable to capture images of the debris flow at night, and even during the day, rain or splashing debris caused water droplets to stick to the camera lens, making some of the images blurry. In addition, the image recording interval was 5 minutes, which was useful for tracking the debris flow but lacking the time resolution to capture changes in the flow field during the development of the debris flow. Future research should shorten the image interval and equip each monitoring station with a wider range of instruments, including flow meters, to support seismic signal analysis and velocity estimation. More observation stations should be set up over a larger area to generate a more

comprehensive dataset. Ultimately, we hope that this study will contribute to a better understanding of the entire debris flow process and, through improvements in seismic signal-based monitoring and analysis, enable a more accurate quantitative reconstruction of the debris flow process, thereby improving the effectiveness of subsequent debris flow detection, early warning, and inversion efforts.

We have used the assumptions of point sources and plane waves to simplify the calculation of the compensation. Theoretically, the compensation should be calculated by integrating over the channel. However, due to variations in the response functions of the point sources at different locations in the channel and factors such as loose surface, meandering flow and varying river width, integration becomes difficult. Therefore, we chose a simplified approach. We assumed a constant propagation velocity and a constant quality factor in the propagation area, ignoring changes in river width, and calculated the weighted travel time from a river section near the monitoring point to the monitoring point itself. The compensation of the propagation effect was then based on the assumption of a plane wave. Since this method is inherently subject to some errors, we adjusted the gain factor to maximize compensation and ensure numerical stability.

6 Conclusions

In this study, a seismic signal-based debris flow monitoring system successfully recorded three debris flow events in Wenchuan, China, on August 19, 2022. Analysis revealed that all three events showed rapid excitation followed by slow attenuation of their seismic signals. Attenuation compensation applied to the second debris flow in Fotangba Gully showed that the kinematic characteristics of the debris flow changed during its progression. By combining seismic signals, video and field investigation analyses, the second debris flow event in Fotangba Gully was reconstructed. The average flow velocity was found to be 7.0 m/s using cross-correlation, which was validated with the Manning formula. Furthermore, a synchronous relationship between PSD and debris flow characteristics was clear under a short period of debris flow events.

The decline of PSD amplitude reflected the decrease of debris flow velocity. Our results are helpful to the reconstruction analysis and inversion of the evolution process of debris flow.

Acknowledgments

This study was financially supported by the National Natural Science Foundation of China (grant nos. U21A2008, 42120104002, and 42271075), the Second Tibetan Plateau Scientific Expedition and Research Program (STEP) (grant no. 2019QZKK0906).

Code/Data availability

All raw data can be provided by the corresponding authors upon request.

Author contributions

The authors of this manuscript entitled “Monitoring, analysis and application of debris flow based on seismic signal” are Yan Yan, Renhe Wang, Cheng Zeng, Yifei Cui, Sheng Hu, Xinglu Wang, and Hui Tang. Yan Yan is the first author and is responsible for Conceptualization, Methodology, Writing-Original draft preparation in this research. Renhe Wang is the second author, is responsible for data organization, validation, and revising the original draft. Cheng Zeng is the third author, responsible for data collection, field investigation, and manuscript revision. Yifei Cui is the fourth author and the corresponding author, is responsible for the Review & Editing, Supervision. Sheng Hu is the fifth author and is responsible for Visualization. Xinglu Wang is responsible for the Investigation, Validation. Hui Tang is the seventh author and is responsible for Writing- Reviewing and Editing.

Competing interests

The authors declare that they have no conflict of interest.

References

Aaron, J., Spielmann, R., McArdell, B. W., Graf, C., 2023. High-Frequency 3D LiDAR Measurements of a Debris Flow: A Novel Method to Investigate the Dynamics of Full-Scale Events in the Field. Geophys. Res. Lett. 50(5), e2022GL102373.

Allstadt, K. E., Farin, M., Iverson, R. M., Obryk, M. K., Kean, J. W., Tsai, V. C., Logan, M., 2020. Measuring basal force fluctuations of debris flows using seismic recordings and empirical green's functions. Journal of Geophysical Research: Earth Surface, 125(9), e2020JF005590.

Andrade, S.D., Almeida, S., Saltos, E., Pacheco, D., Hernandez, S., Acero, W., 2022. A simple and general methodology to calibrate seismic instruments for debris flow quantification: application to Cotopaxi and Tungurahua volcanoes (Ecuador). Landslides 19(3), 747-759.

Arattano, M., 1999. On the use of seismic detectors as monitoring and warning systems for debris flows. Nat. Hazards 20(2-3), 197-213.

Arattano, M., Marchi, L., 2005. Measurements of debris flow velocity through cross-correlation of instrumentation data. Nat. Hazards Earth Syst. Sci. 5(1), 137-142.

Arattano, M., Marchi, L., 2008. Systems and sensors for debris-flow monitoring and warning. Sensors 8(4), 2436-2452.

Beason, S.R., Legg, N.T., Kenyon, T.R., Jost, R.P., 2021. Forecasting and seismic detection of proglacial debris flows at Mount Rainier National Park, Washington, USA. Environ. Eng. Geosci. 27(1), 57-72.

Belli, G., Marchetti, E., Walter, F., Gheri, D., 2025. Infrasound unmasks flow turbulence as an additional seismic source in debris flows. Geophysical Research Letters, 52(8), e2025GL116107.

Belli, G., Walter, F., McArdell, B., Gheri, D., Marchetti, E., 2022. Infrasonic and seismic analysis of debris‐flow events at Illgraben (Switzerland): Relating signal features to flow parameters and to the seismo‐acoustic source mechanism. J. Geophys. Res.-Earth Surf. 127(6), e2021JF006576.

Burtin, A., Bollinger, L., Cattin, R., Vergne, J., Nábělek, J.L., 2009. Spatiotemporal sequence of Himalayan debris flow from analysis of high-frequency seismic noise. J. Geophys. Res. 114, F04009.

Burtin, A., Hovius, N., McArdell, B. W., Turowski, J. M., Vergne, J., (2014). Seismic constraints on dynamic links between geomorphic processes and routing of sediment in a steep mountain catchment. Earth Surface Dynamics, 2(1), 21-33.

Cao, C., Yu, B., Ma, E.L., Liu, S., 2019. Study on debris flow in Fongtuba Gully after the earthquake at Wenchuan County of Sichuan Province. Journal of Sediment Research 44(1), 38-43 (in Chinese).

Chang, M., Liu, Y., Zhou, C., Che, H., 2020. Hazard assessment of a catastrophic mine waste debris flow of Hou Gully, Shimian, China. Engineering Geology, 275, 105733.

Chen, X., Cui, P., You, Y., Chen, J., Li, D., 2015. Engineering measures for debris flow hazard mitigation in the Wenchuan earthquake area. Engineering Geology, 194, 73-85.

Comiti, F., Marchi, L., Macconi, P., Arattano, M., Bertoldi, G., Borga, M., Brardinoni, F., Cavalli, M., D'Agostino, V., Pennna, D., Theule, J., 2014. A new monitoring station for debris flows in

the European Alps: first observations in the Gadria basin. Nat. Hazards 73, 1175-1198.
Coviello, V., Arattano, M., Turconi, L., 2015. Detecting torrential processes from a distance with a seismic monitoring network. Nat. Hazards 78, 2055-2080.
Crowley, J. K., Hubbard, B. E., Mars, J. C., 2003. Analysis of potential debris flow source areas on Mount Shasta, California, by using airborne and satellite remote sensing data. Remote Sensing of Environment, 87(2-3), 345-358.
Cui, P., Guo, X., Yan, Y., Li, Y., Ge, Y., 2018. Real-time observation of an active debris flow watershed in the Wenchuan Earthquake area. Geomorphology 321, 153-166.
Cui, P., Zhou, G.G., Zhu, X.H., Zhang, J.Q., 2013. Scale amplification of natural debris flows caused by cascading landslide dam failures. Geomorphology 182, 173-189.
Deparis, J., Jongmans, D., Cotton, F., Baillet, L., Thouvenot, F., Hantz, D., 2008. Analysis of rock-fall and rock-fall avalanche seismograms in the French Alps. Bull. Seismol. Soc. Amer. 98(4), 1781-1796.
Farin, M., Tsai, V. C., Lamb, M. P., Allstadt, K. E., 2019. A physical model of the high-frequency seismic signal generated by debris flows. Earth Surface Processes and Landforms, 44(13), 2529-2543.
Fu, J., Wang, X., Li, Z., Meng, H., Wang, J., Wang, W., Tang, C., 2020. Automatic phase-picking method for detecting earthquakes based on the signal-to-noise-ratio concept. Seismological Research Letters, 91(1), 334-342.
Fuchs, F., Lenhardt, W., Bokelmann, G., AlpArray Working Group, 2018. Seismic detection of rockslides at regional scale: examples from the Eastern Alps and feasibility of kurtosis-based event location. Earth Surf. Dyn. 6(4), 955-970.
Futterman, W. I., 1962. Dispersive body waves. J. Geophys. Res. 67(13), 5279-5291.
Guo, N., Zhou, X., Xu, K., Wang, Y., Lyu, J, Duan, M., 2023. Near-surface *Q*-value survey method based on uphole with hammer excitation and receiving using multi-stage geophones on wells. Oil Geophysical Prospecting 58(2), 295-304 (in Chinese).
Guo, X., Cui, P., Li, Y., Zou, Q., Kong, Y., 2016. The formation and development of debris flows in large watersheds after the 2008 Wenchuan Earthquake. Landslides 13, 25-37.
He, K., Liu, B., Hu, X., Zhou, R., Xi, C., Ma, G., Luo, G., 2022. Rapid characterization of landslide-debris flow chains of geologic hazards using multi-method investigation: Case study of the Tiejiangwan LDC. Rock Mechanics and Rock Engineering, 55(8), 5183-5208.
Huang, C. J., Chu, C. R., Tien, T. M., Yin, H. Y., Chen, P. S., 2012. Calibration and deployment of a fiber-optic sensing system for monitoring debris flows. Sensors 12(5), 5835-5849.
Hübl, J., Schimmel, A., Kogelnig, A., Suriñach, E., Vilajosana, I., McArdell, B.W., 2013. A review on acoustic monitoring of debris flow. International Journal of Safety and Security Engineering 3(2), 105-115.
Hürlimann, M., Coviello, V., Bel, C., Guo, X., Berti, M., Graf, C., Hürl, J., Miyata, S., Smith, J.B., Yin, H.-Y., 2019. Debris-flow monitoring and warning: Review and examples. Earth-Sci. Rev. 199, 102981.
Iverson, R. M., 2015. Scaling and design of landslide and debris-flow experiments. Geomorphology, 244, 9-20.
Iverson, R.M., 1997. The physics of debris flows. Rev. Geophys. 35(3), 245-296.

935 Kean, J. W., Coe, J. A., Coviello, V., Smith, J. B., McCoy, S. W., Arattano, M., 2015. Estimating
936 rates of debris flow entrainment from ground vibrations. Geophysical Research Letters, 42(15),
937 6365-6372.
938 Kean, J. W., Staley, D. M., Leeper, R. J., Schmidt, K. M., Gartner, J. E., 2012. A low‐cost method
939 to measure the timing of postfire flash floods and debris flows relative to rainfall. Water Resour.
940 Res. 48(5), W05516.
941 Kean, J.W., Staley, D.M., Lancaster, J.T., Rengers, F.K., Swanson, B.J., Coe, J.A., Hernandez, J.L.,
942 Sigman, A.J., Allstadt, K.E., Lindsay, D.N., 2019. Inundation, flow dynamics, and damage in
943 the 9 January 2018 Montecito debris-flow event, California, USA: Opportunities and
944 challenges for post-wildfire risk assessment. Geosphere 15(4), 1140-1163.
945 Kjartansson, E., 1979. Constant Q‐wave propagation and attenuation. J. Geophys. Res.-Solid
946 Earth 84(B9), 4737-4748.
947 Kogelnig, A., Hübl, J., Suriñach, E., Vilajosana, I., McArdell, B.W., 2014. Infrasound produced by
948 debris flow: propagation and frequency content evolution. Nat. Hazards 70, 1713-1733.
949 Lai, V.H., Tsai, V.C., Lamb, M.P., Ulizio, T.P., Beer, A.R., 2018. The seismic signature of debris
950 flows: Flow mechanics and early warning at Montecito, California. Geophys. Res. Lett. 45(11),
951 5528-5535.
952 Li, Z., Huang, X., Xu, Q., Yu, D., Fan, J., Qiao, X., 2017. Dynamics of the Wulong landslide
953 revealed by broadband seismic records. Earth, Planets and Space 69, 1-10.
954 Liang, X., Segoni, S., Yin, K., Du, J., Chai, B., Tofani, V., Casagli, N., 2022. Characteristics of
955 landslides and debris flows triggered by extreme rainfall in Daoshi Town during the 2019
956 Typhoon Lekima, Zhejiang Province, China. Landslides, 19(7), 1735-1749.
957 Liu C., Feng X., Zhang J., 2013. A stable inverse Q filtering using the iterative filtering method. Oil
958 Geophysical Prospecting 48(6), 890-895 (in Chinese).
959 Marchetti, E., Walter, F., Barfucci, G., Genco, R., Wenner, M., Ripepe, M., McArdell, B., Price, C.,
960 2019. Infrasound array analysis of debris flow activity and implication for early warning. J.
961 Geophys. Res. 124(2), 567-587.
962 Marchi, L., Arattano, M., Deganutti, A. M., 2002. Ten years of debris-flow monitoring in the
963 Moscardo Torrent (Italian Alps). Geomorphology, 46(1-2), 1-17.
964 McArdell, B. W., Bartelt, P., Kowalski, J., 2007. Field observations of basal forces and fluid pore
965 pressure in a debris flow. Geophys. Res. Lett. 34(7), L07406.
966 McCoy, S. W., Kean, J. W., Coe, J. A., Staley, D. M., Wasklewicz, T. A., Tucker, G. E., 2010.
967 Evolution of a natural debris flow: In situ measurements of flow dynamics, video imagery, and
968 terrestrial laser scanning. Geology 38(8), 735-738.
969 Nagl, G., Hübl, J. 2017. A check-dam to measure debris flow-structure interactions in the Gadria
970 torrent. In: M., Mikoš, Ž., Arbanas, Y., Yin, K., Sassa (eds.), Advancing Culture of Living with
971 Landslides-Volume 5: Landslides in Different Environments. Springer International Publishing,
972 pp. 465-471.
973 Rickenmann, D., 1999. Empirical relationships for debris flows. Nat. Hazards 19, 47-77.
974 Schenato, L., Pasuto, A., 2021. On the Use of Optical Fiber Sensors for Debris Flow Monitoring: A
975 Review of Recent Achievements. Belt and Road Webinar Series on Geotechnics, Energy and
976 Environment pp. 60-70.

977 Schimmel, A., Coviello, V., Comiti, F., 2022. Debris flow velocity and volume estimations based
978 on seismic data. Nat. Hazards Earth Syst. Sci. 22(6), 1955-1968.
979 Schimmel, A., Hübl, J., 2016. Automatic detection of debris flows and debris floods based on a
980 combination of infrasound and seismic signals. Landslides 13, 1181-1196.
981 Schneider, D., Bartelt, P., Caplan‐Auerbach, J., Christen, M., Huggel, C., McArdell, B.W., 2010.
982 Insights into rock-ice avalanche dynamics by combined analysis of seismic recordings and a
983 numerical avalanche model. J. Geophys. Res. 115, F04026.
984 Strick, E., 1967. The determination of Q, dynamic viscosity and transient creep curves from wave
985 propagation measurements. Geophys. J. Int. 13(1-3), 197-218.
986 Suwa, H., Okano, K., Kanno, T., 2009. Behavior of debris flows monitored on test slopes of
987 Kamikamihorizawa Creek, Mount Yakedake, Japan. International Journal of Erosion Control
988 Engineering 2(2), 33-45.
989 Tang, C., Rengers, N.V., Van Asch, T.W., Yang, Y.H., Wang, G.F., 2011. Triggering conditions and
990 depositional characteristics of a disastrous debris flow event in Zhouqu city, Gansu Province,
991 northwestern China. Nat. Hazards Earth Syst. Sci. 11(11), 2903-2912.
992 Tecca, P.R., Galgaro, A., Genevois, R., Deganutti, A.M., 2003. Development of a remotely
993 controlled debris flow observation system in the Dolomites (Acquabona, Italy). Hydrol.
994 Process. 17(9), 1771-1784.
995 Tsai, V. C., Minchew, B., Lamb, M. P., & Ampuero, J.-P., 2012. A physical model for seismic noise
996 generation from sediment transport in rivers. Geophysical Research Letters, 39(2), L02404.
997 Turbessi, L., Taboni, B., Umili, G., Fubelli, G., Ferrero, A. M., 2025. Modeling Debris Flow Events
998 in the Rio Inferno Watershed (Italy) Through UAV-Based Geomorphological Survey and
999 Rainfall Data Analysis. Sensors, 25(7), 1980.
1000 Van Herwijnen, A., Schweizer, J., 2011. Monitoring avalanche activity using a seismic sensor. Cold
1001 Reg. Sci. Tech. 69(2-3), 165-176.
1002 Vilajosana, I., Suriñach, E., Abellán, A., Khazaradze, G., Garcia, D., Llosa, J., 2008. Rockfall
1003 induced seismic signals: case study in Montserrat, Catalonia. Nat. Hazards Earth Syst. Sci. 8(4),
1004 805-812.
1005 Walter, F., Burtin, A., McArdell, B.W., Hovius, N., Weder, B., Turowski, J.M., 2017. Testing seismic
1006 amplitude source location for fast debris-flow detection at Illgraben, Switzerland. Nat. Hazards
1007 Earth Syst. Sci. 17(6), 939-955.
1008 Wang, Y., 2002. A stable and efficient approach of inverse Q filtering. Geophysics, 67(2), 657-663.
1009 Xu, M.D., Feng, Q.H., 1979. Roughness of debris flows. Proceeding of the First Conference of
1010 Chinese Research of Debris Flows, pp. 51-52 (in Chinese).
1011 Yan, Y., Cui, P., Chen, S., Chen, X., Chen, H., Chien, Y., 2017. Characteristics and interpretation of
1012 the seismic signal of a field-scale landslide dam failure experiment. J. Mt. Sci. 14, 219-236.
1013 Yan, Y., Cui, Y., Huang, X., Zhou, J., Zhang, W., Yin, S., Guo, J., Hu, S., 2022. Combining seismic
1014 signal dynamic inversion and numerical modeling improves landslide process reconstruction.
1015 Earth Surf. Dynam. 10, 1233–1252.
1016 Yan, Y., Cui, Y., Liu, D., Tang, H., Li, Y., Tian, X., Zhang, L., Hu, S., 2021. Seismic signal
1017 characteristics and interpretation of the 2020 “6.17” Danba landslide dam failure hazard chain
1018 process. Landslides 18, 2175-2192.

Yan, Y., Cui, Y., Tian, X., Hu, S., Guo, J., Wang, Z., Yin S., Liao, L., 2020. Seismic signal recognition and interpretation of the 2019 “7.23” Shuicheng landslide by seismogram stations. Landslides 17, 1191-1206.

Yan, Y., Tang, H., Hu, K., Turowski, J. M., Wei, F., 2023. Deriving debris-flow dynamics from real-time impact-force measurements. J. Geophys. Res. 128, e2022JF006715.

Yan, Y., Tang, H., Zhou, K., Turowski, J. M., Cui, Y., & Xiang, B. (2025). Statistical characteristics of basal forces generated by experimental debris flows. J. Geophys. Res.-Solid Earth 130, e2024JB030027. https://doi.org/10.1029/2024JB030027.

Yang, H., Haque, E., & Song, K., 2021. Experimental study on the effects of physical conditions on the interaction between debris flow and baffles. Physics of Fluids, 33(5).

Yu, G., Lim, S.Y., 2003. Modified Manning formula for flow in alluvial channels with sand-beds. J. Hydraul. Res. 41(6), 597-608.

Zhang, W., Chen, J., Ma, J., Cao, C., Yin, H., Wang, J., & Han, B., 2023. Evolution of sediment after a decade of the Wenchuan earthquake: a case study in a protected debris flow catchment in Wenchuan County, China. Acta Geotechnica, 18(7), 3905-3926.

Zhang, X., Tang, C., Li, N., Xiong, J., Chen, M., Li, M., Tang, C., 2022. Investigation of the 2019 Wenchuan County debris flow disaster suggests nonuniform spatial and temporal post-seismic debris flow evolution patterns. Landslides, 19(8), 1935-1956.

Zhang, Z., 2021. Study on the inversion of dynamic parameters of landslides and debris flows based on seismic signals. University of Chinese Academy of Sciences (in Chinese).

Zhang, Z., Walter, F., McArdell, B. W., Haas, T., Wenner, M., Chmiel, M., He, S., 2021a. Analyzing bulk flow characteristics of debris flows using their high frequency seismic signature. J. Geophys. Res.-Solid Earth 126(12), e2021JB022755.

Zhang, Z., Walter, F., McArdell, B. W., Wenner, M., Chmiel, M., de Haas, T., He, S., 2021b. Insights from the particle impact model into the high-frequency seismic signature of debris flows. Geophysical Research Letters, 48(1), e2020GL088994.